Research Square

Preprints are preliminary reports that have not undergone peer review.
They should not be considered conclusive, used to inform clinical practice,
or referenced by the media as validated information.

Uncertainty-aware heatwave hazard zoning for India from two gridded temperature records

Ajay Sharma

ajay.sharma@globeir.com

Soban Singh Jeena University

Vipin Chandra Lal

University of Delhi

Gajendra Singh Sisodiya

University of Pécs

Research Article

Keywords:

Posted Date: November 25th, 2026

DOI: https://doi.org/10.21203/rs.3.rs-11616642/v1

License: This work is licensed under a Creative Commons Attribution 4.0 International License.
Read Full License

Additional Declarations: Competing interest reported. A.S. is the founder, Chief Executive Officer and Managing Director of Globeir Private Limited, which funded this work. V.C.L. and G.S.S. declare no financial or non-financial competing interests.

Uncertainty-aware heatwave hazard zoning for India from two gridded temperature records

Ajay Sharma[1]*, Vipin Chandra Lal[2], Gajendra Singh Sisodiya[3]

[1] Soban Singh Jeena University, Almora, Uttarakhand, India. [2] Dr. Bhim Rao Ambedkar College, University of Delhi, Delhi, India. [3] Institute of Geography and Earth Sciences, University of Pécs, 7622 Pécs, Hungary.

* Corresponding author: Ajay Sharma (ajay.sharma@globeir.com)

ORCID: Ajay Sharma https://orcid.org/0009-0001-6077-9875; Vipin Chandra Lal https://orcid.org/0009-0003-1883-1582; Gajendra Singh Sisodiya https://orcid.org/0009-0006-4118-7491

E-mail: Ajay Sharma ajay.sharma@globeir.com; Vipin Chandra Lal vipin.chandralal30@gmail.com; Gajendra Singh Sisodiya gajendra.singh11@edu.pte.hu

Abstract

India's heat planning rests on a Core Heat Wave Zone published as a list of states and subdivisions, with no threshold, method or uncertainty. We zoned heatwave hazard over India's lowland, 1951–2025, from two gridded records: IMD's 1° station-based grid and 0.1° ERA5-Land aligned to it. A tiered product separates an occurrence zone (31% of the lowland) from a concentration core (19%; robust core 13%) whose cells keep their top-quartile rank under block-bootstrap resampling of both datasets. The official list is a near-optimal coverage zone, capturing 95% of heatwave days on 74% of the area; the core holds 54% on 19%, but out of sample matches a zone of past heatwave days. Places divide weakly into higher- and lower-hazard regimes, which location predicts as well as terrain, irrigation and rainfall. Since 1951–1980 the core shifted west beyond resampling noise, but not from 1966–1995. A GeoPackage with district summaries is released.

Introduction

Heatwaves are India's most widespread meteorological hazard, and the country's heat planning rests on a geographical construct: the Core Heat Wave Zone of the India Meteorological Department (IMD). IMD's 2020 hot-season outlook named it as fifteen states and three meteorological subdivisions[1]; the term comes from IMD's station climatology of heatwaves[2], which builds on earlier station analyses[3], but the list has no published threshold, method or uncertainty, and the most recent outlook does not use it[4]. National guidelines ask states to set local heat thresholds[5], which only ten of 37 reviewed heat action plans have done[6]. Where heatwave hazard is concentrated, and how a zone that guides warnings and funds should be drawn, are therefore geospatial questions with operational consequences.

Heatwave frequency and duration have risen most over north-western and central India[7,8], heatwaves now reach the west coast, the north-east and the hills[9], heatwaves have become more frequent in the south-east and less frequent in the east[10], and gridded hotspot maps show the area of heatwave hotspots

growing about 1.5-fold between 1981–2000 and 2001–2020[11]. Indian heatwaves form at least two spatial types with different mechanisms, one over north-central India linked to a wave train from the North Atlantic and one along the east coast[12], and dry and moist heatwaves favour different intraseasonal phases[13]. Hazard zonations exist from station data[14] and at district scale[15], and regionalisations by clustering exist for heatwaves in Europe, South America and China[16–19].

Three geoinformatics gaps remain. First, no zoning of Indian heatwave hazard states its uncertainty, separates where heatwaves occur from where they are concentrated, or is evaluated as a decision product with out-of-sample tests. Second, IMD's criteria were written for stations and are applied to grids without testing how their absolute and relative rules and their terrain classes shape the result. Third, the two long gridded records — IMD's station-based 1° grid[20] and the 0.1° ERA5-Land reanalysis[21] — differ in resolution and in their trends, so a zoning must say which source carries which information.

This study asks four questions, each answered by one objective, using stability-tested clustering, random forests under spatial cross-validation and bootstrap spatial statistics. First, how is heatwave hazard distributed over India's lowland, and how well do the region layers used for reporting capture it? We map IMD-criterion heatwave metrics from IMD 1° and trend-aligned ERA5-Land 0.1° data and test IMD's regions and subdivisions, climate groups and the Core Heat Wave Zone against random partitions of the same size. Second, do places fall into distinct heatwave regimes, and how are they associated with terrain, coast distance, irrigation and rainfall? We cluster multi-metric heatwave climatologies with year-bootstrap stability and unimodal null tests, and predict the regimes from covariates against location baselines. Third, where is the core of heatwave hazard, how certain is it, and how does it compare with IMD's list? We build tiered zones — an occurrence zone, a concentration core with bootstrap membership frequencies that must hold in both datasets, and a Getis–Ord hotspot zone — and evaluate them as decision products with concentration curves, recall, equal-area alternatives, out-of-sample tests and a sensitivity matrix. Fourth, has the core changed since the mid-twentieth century, and how can zoning reach planners? We compare the core between periods against the change expected from resampling alone and translate every product to districts and subdivisions. The study area is shown in Fig. 1 and the workflow in Fig. 2.

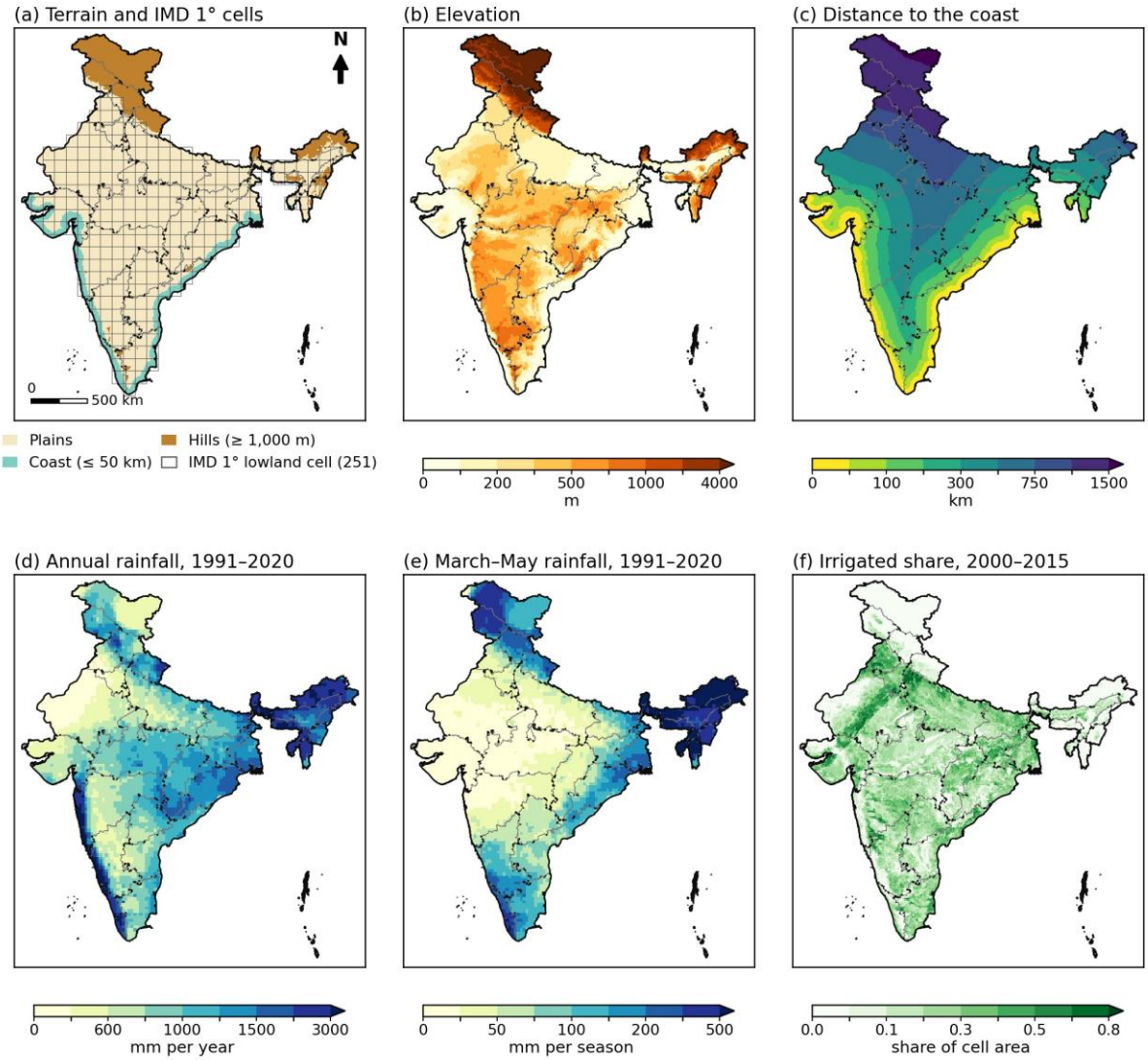

Fig. 1 | Study area and covariates. (a) Terrain classes (plains; coast within 50 km of the sea; hills at or above 1,000 m, not analysed) and the 251 IMD 1° lowland cells analysed; (b) elevation; (c) distance to the coast; (d) annual and (e) March–May rainfall, 1991–2020 (IMD 0.25°); (f) irrigated share of each 0.1° cell, 2000–2015. Survey of India outline.

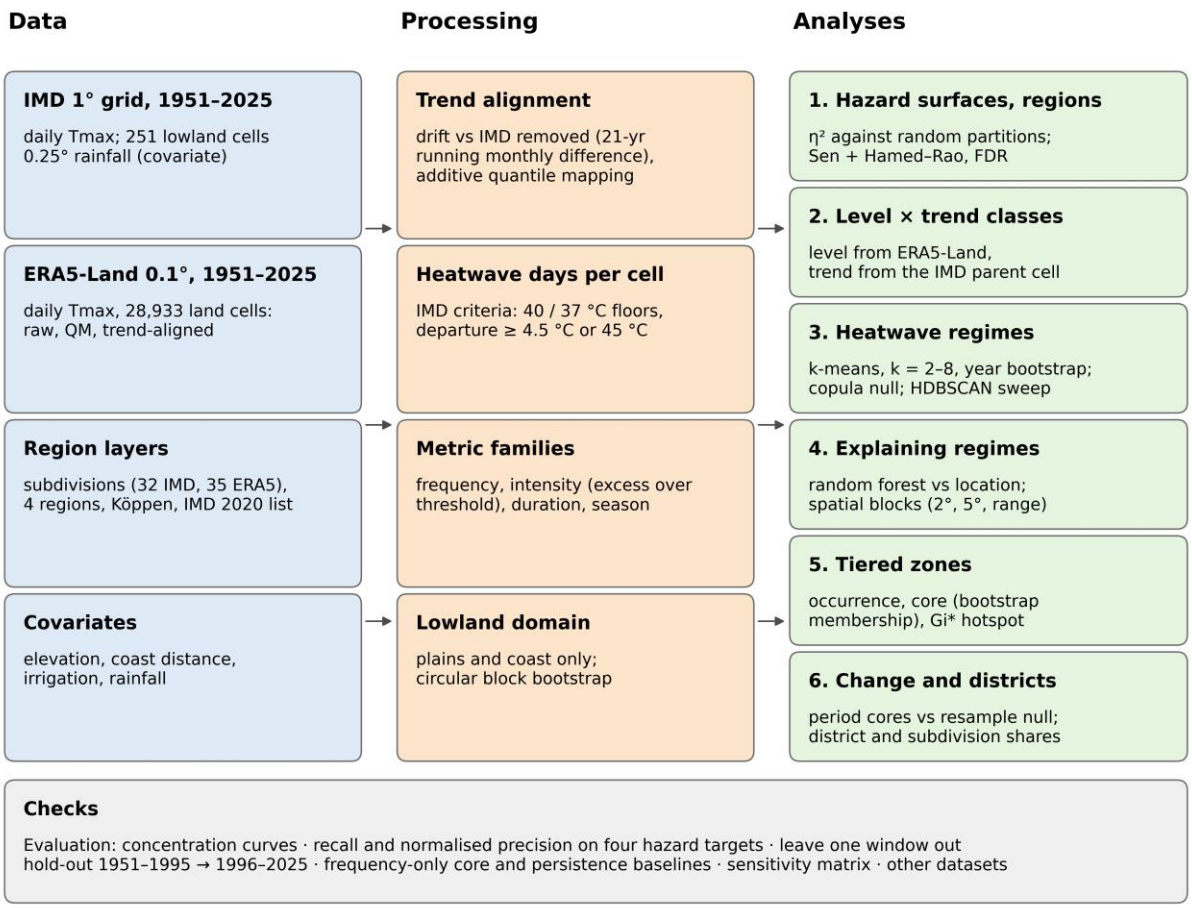

Fig. 2 | Workflow. Data, processing, the six analyses and the checks applied to the zones.

Results

Heatwave hazard surfaces from two gridded sources

Heatwave days per year over 1951–2025 peak on the Indo-Gangetic plain from Punjab to East Uttar Pradesh and in Jharkhand in both datasets (at least 2.6 days a year, against lowland means of 1.71 in ERA5-Land and 1.31 in IMD); ERA5-Land also has many in Gangetic West Bengal and Vidarbha, where IMD has fewer (Fig. 3a,b). The two IMD rules trigger different heatwave days: over the lowland, 19% of heatwave days meet only the plains rule of 45 °C, but 27% in West Rajasthan, 37% in East Rajasthan and 53% in Vidarbha, where Tmax is high but its departure from normal small (Fig. 3c). Measured as the excess over the threshold each day had to reach, intensity is highest in the east, from Gangetic West Bengal and Jharkhand to Odisha (Fig. 3d). Heatwaves occur in at least one year in three over the Indo-Gangetic plain, Jharkhand and much of Rajasthan (Fig. 3e). The two datasets agree on this pattern but not on its change: aligned ERA5-Land has more lowland heatwave days than IMD in 1951–1965 (2.22 against 0.91 a year) and fewer in 2011–2025 (1.42 against 1.48), because the alignment fixes monthly mean trends at 1° but not the tails (Fig. 3f; Supplementary Table 1). We therefore take spatial pattern from both datasets and change from IMD.

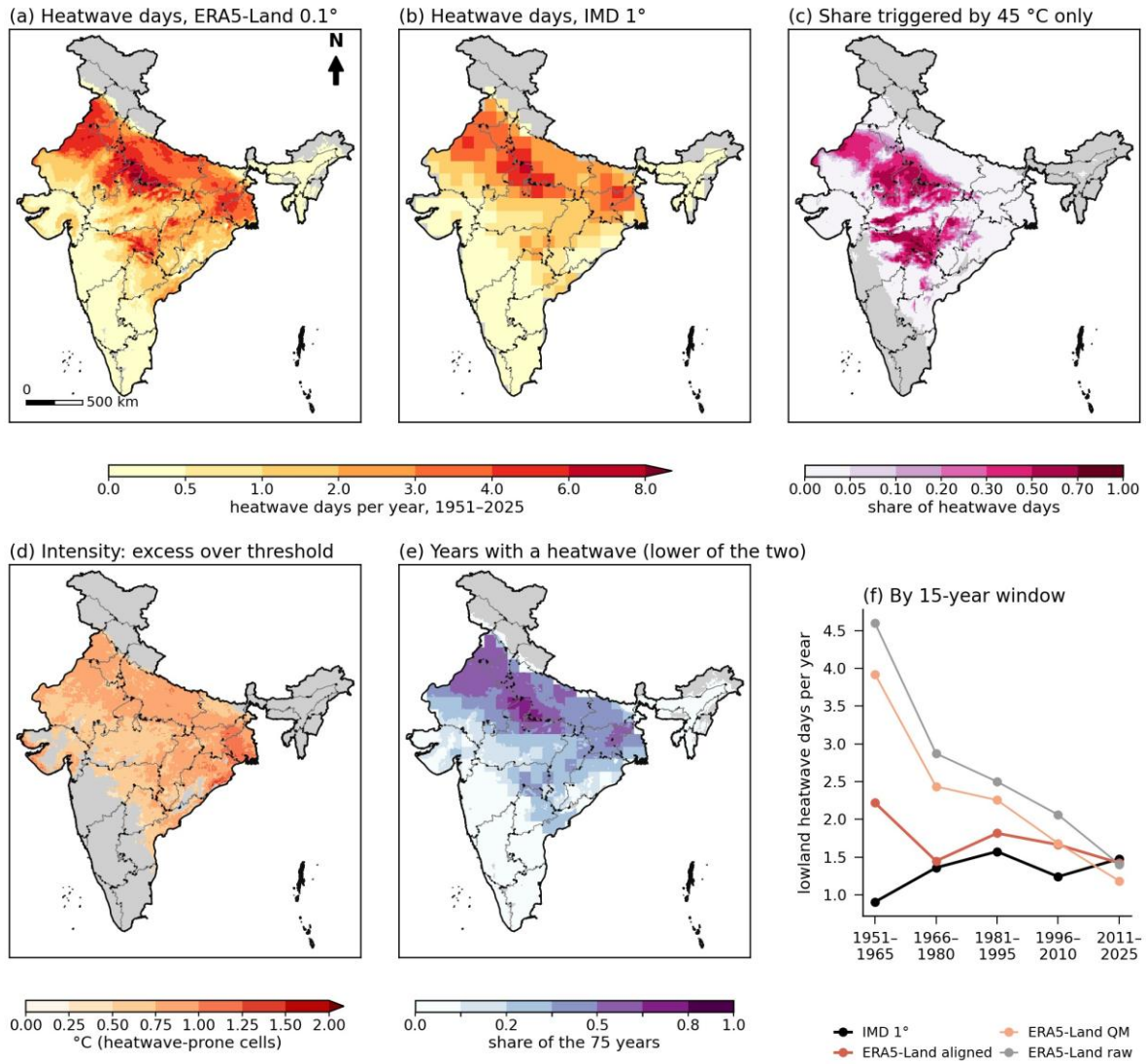

Fig. 3 | Heatwave hazard surfaces of India's lowland, 1951–2025. (a) Heatwave days per year (IMD criteria) in trend-aligned ERA5-Land 0.1° and (b) IMD 1°. (c) Share of heatwave days that meet only the plains rule of 45 °C. (d) Intensity: mean excess of Tmax over the threshold that the day had to reach, heatwave-prone cells. (e) Share of years with a heatwave, the lower of the two datasets. (f) Lowland heatwave days per year by 15-year window in IMD and three versions of ERA5-Land. Hills (grey) are not analysed. Survey of India outline.

Subdivisions and climate groups capture heatwave days no better than chance partitions

How much of the heatwave pattern a region layer captures depends on its number of units, so each layer was compared with random compact partitions of the lowland into the same number of regions (Fig. 4a; Supplementary Table 2). IMD's 32–35 subdivisions capture 0.63 (IMD) and 0.60 (ERA5-Land) of the variance of heatwave days, less than random partitions (0.67–0.77 and 0.64–0.69), and the Köppen–Geiger groups also fall below chance (0.18 and 0.11). IMD's four homogeneous regions (0.34 and 0.30) and the split into inside and outside the Core Heat Wave Zone (0.21 and 0.20) beat chance for heatwave days, but not for intensity or the longest event, whereas the Köppen–Geiger groups beat chance for the longest event and the season span (Supplementary Table 2). The spread of subdivision trends exceeds

that expected with no trend anywhere (van Belle–Hughes bootstrap $p = 0.028$ and $p = 0.037$ for heatwave days), but after false-discovery control ($q < 0.10$) over all 40 tests only IMD's results remain (23 and 0 of 40; Supplementary Table 3). Both datasets agree on rising heatwave days in West Rajasthan (+0.39 and +0.25 days per decade) and falling ones in Gangetic West Bengal (−0.17 and −0.28; Fig. 4b; Supplementary Table 4), and on an earlier first heatwave day in 5 north-western subdivisions (East Rajasthan, Haryana-Chandigarh-Delhi, West Madhya Pradesh, West Rajasthan and West Uttar Pradesh). In IMD the earlier onset persists after accounting for the rise in heatwave days in 4 subdivisions at $q < 0.10$ (East Rajasthan, West Uttar Pradesh, Haryana-Chandigarh-Delhi and Punjab; 6 at $p < 0.05$ without correction). Percentile-based heatwave days (TX90) rise significantly in 20 IMD subdivisions across the peninsula and central India, including southern subdivisions where IMD-criterion heatwave days hardly occur, so the two definitions describe different hazards in the south. Combining ERA5-Land's level with IMD's trend, 4.5% of the lowland has many heatwave days and an increase, 18.4% many and no detectable change and 1.8% many and a decrease (Supplementary Table 5); 5.1%, whose 1° parent is not an IMD lowland cell, has no trend class. ERA5-Land's own trend class agrees with IMD's in 89% of the area, almost all of it without a detectable change in either (Cohen's $\kappa = 0.17$).

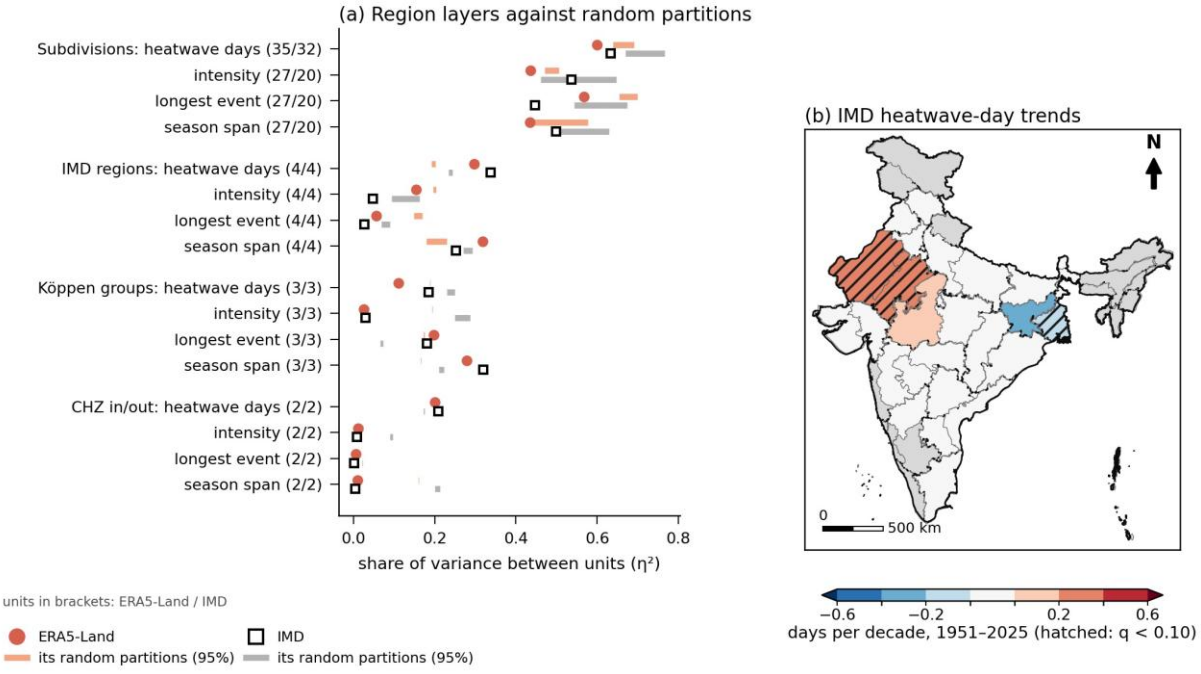

Fig. 4 | Region layers and subdivision trends. (a) Share of the area-weighted variance of per-cell climatology lying between units (η^2) for each layer and metric (number of units in brackets), trend-aligned ERA5-Land (dots) and IMD (squares), against the 95% range of 50 random compact partitions of the lowland into the same number of regions (grey). (b) Sen trend of heatwave days per subdivision in IMD 1°, 1951–2025; hatched where $q < 0.10$ (Benjamini–Hochberg within the layer). Survey of India outline.

A higher- and a lower-hazard regime of places

Clustering the heatwave climatologies of the 16,394 heatwave-prone cells gives two regimes as the most stable solution in both datasets (Fig. 5): in ERA5-Land every regime keeps a mean Jaccard of 0.76–0.83 under resampled years, and no solution with three or more regimes reaches 0.75 (mean 0.52 at $k = 3$); in IMD, $k = 2$ is also the most stable solution, although one of its regimes keeps only 0.71 (0.71–0.80; Supplementary Table 6). The gap criterion is not met for any $k \leq 9$. The structure is weak: the silhouette at $k = 2$ is 0.32, in the range of weak structure (0.26–0.50), though above that of Gaussian and Gaussian-copula surrogates with the same correlations and no clusters (at most 0.26 and 0.27). Regime 1 (1.13 million km²; mainly East Uttar Pradesh, Chhattisgarh, West Uttar Pradesh and Odisha) has 3.4 heatwave days a year, longer events (longest 4.6 days), a longer heatwave season (17 days) and greater intensity (0.84 °C above the threshold); regime 2 (0.72 million km²; mainly West Madhya Pradesh, West Rajasthan, East Rajasthan, East Madhya Pradesh, Telangana and Gujarat Region) has 1.3 days a year, 3.3-day longest events and 0.66 °C. The regimes differ in the same direction in every family (Fig. 5c), and the first principal component carries 47% of the feature variance, so they divide a severity gradient — a higher- and a lower-hazard regime — rather than separate distinct kinds of heatwave. Both regimes have about one heatwave day in five triggered only by the 45 °C rule (20% and 18%). The regimes agree moderately with IMD's (adjusted Rand index 0.43) and with quantile-mapped ERA5-Land (0.52; Supplementary Fig. 1), less with raw data (0.29) and the percentile definition (0.30; Supplementary Table 7); HDBSCAN finds two dense groups only with small minimum-sample settings (Supplementary Table 8).

Location predicts the regimes as well as the covariates do. Under 2° and 5° spatial blocks, latitude and longitude alone predict the held-out regime on the plains (balanced accuracy of the better location model 0.87 and 0.80) as well as or better than elevation, coast distance, irrigation and rainfall (0.84 and 0.77; chance 0.50; means over ten random offsets of the block grid; Supplementary Fig. 2; Supplementary Table 9). Blocks at the 1,575 km range of the regime pattern (15°) leave only 5 blocks on the plains, and the largest fold holds up to 91% of the cells, so the estimates vary widely between offsets (covariates 0.51–0.75, location 0.61–0.73). The covariates therefore add no demonstrable predictive information beyond location; coast distance and rainfall, which co-varies with heatwaves through pre-monsoon showers, carry most of the permutation importance, which describes the fitted forest rather than a cause.

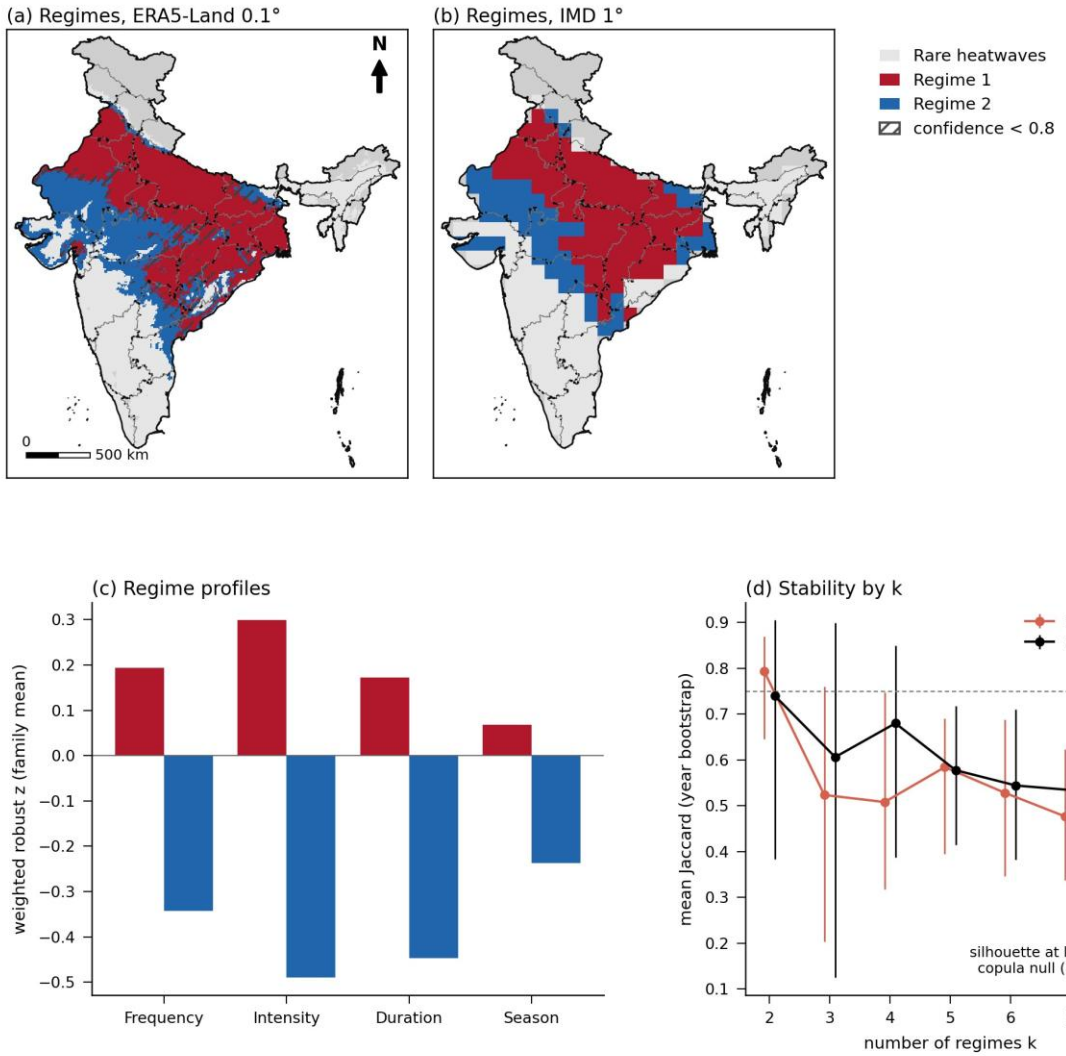

Fig. 5 | Heatwave regimes of places. (a) Regimes of heatwave-prone lowland cells in trend-aligned ERA5-Land 0.1° (hatched: the cell keeps its regime in fewer than 80% of 300 year-bootstrap samples) and (b) in IMD 1°; other lowland cells have rare heatwaves. (c) Regime profiles: mean weighted robust z of each metric family (each family has total weight one). (d) Mean Jaccard similarity of the regimes to the reference solution under 100 circular block bootstrap samples of the years (95% range), by number of regimes; dashed: the 0.75 rule. Survey of India outline.

Tiered heatwave zones with bootstrap membership

The three zones answer different questions (Fig. 6). The occurrence zone (30.8% of the lowland) holds cells with a heatwave in at least one year in three in both datasets. The concentration core (19.5%) holds cells in the top quartile of the frequency score with a bootstrap membership of at least 0.5 in both datasets, and the robust core (13.4%) those at 0.9 or more; the Getis–Ord hotspot zone covers 21.8% and overlaps the core with a Jaccard of 0.74. The core lies on the Indo-Gangetic plain from Punjab to Bihar, in West and East Rajasthan, in the two Madhya Pradesh subdivisions and in Jharkhand — East Uttar Pradesh 19%, West Uttar Pradesh 15%, West Rajasthan 13%, Jharkhand 9% and East Rajasthan 8% of its area — and entirely within IMD's list (100% of its area). Agreement between datasets is partial: the cells with a membership of at least 0.5 overlap with a Jaccard of 0.64 (0.60 at 0.9; rank correlation

0.86), and the robust core falls in 47 IMD 1° boxes, so its outline inherits IMD's resolution. Of 732 districts, 236 have at least half their lowland in the occurrence zone and 160 in the core (Fig. 6d; Supplementary Table 10).

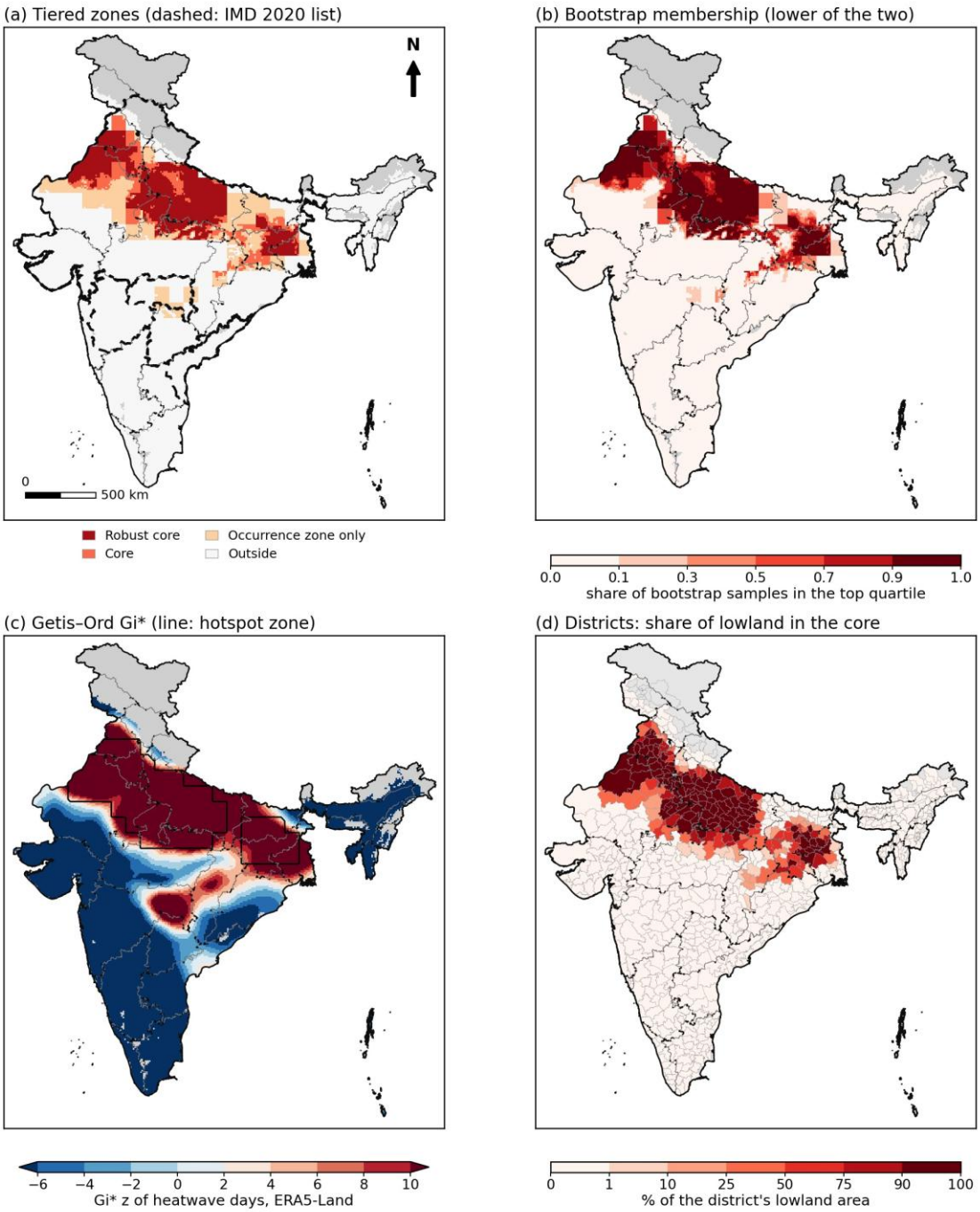

Fig. 6 | Tiered heatwave zones. (a) Robust core (bootstrap membership ≥ 0.9 in both datasets), core (≥ 0.5 in both), occurrence zone only (a heatwave in at least one year in three in both) and the rest of the lowland; dashed: IMD's 2020 Core Heat Wave Zone. (b) Bootstrap membership frequency, the lower of trend-aligned ERA5-Land and IMD (1° parent). (c) Getis–Ord Gi∗ z of heatwave days (ERA5-Land, 100 km); line: hotspot zone ($q < 0.05$ in both datasets). (d) Share of each district's lowland area in the core. Hills are not analysed. Survey of India outline.

Zones as decision products

Heatwave days are unevenly spread (Gini 0.56 in IMD, 0.55 in ERA5-Land), and every zone sits close to the concentration curve (Fig. 7a; Table 1). IMD's list covers 74% of the lowland and captures 95% of IMD heatwave days and 98% of severe ones, a precision of 0.96 of the best zone of its size: as a coverage zone it is near-optimal. The core holds 54% of IMD heatwave days on 19% of the lowland, close to the best possible for its size (normalised precision 0.97), and the occurrence zone 75% on 31% (1.00). A plain threshold of three heatwave days a year does as well in sample, because it is the in-sample optimum for ERA5-Land by construction. Adding intensity, duration and season to the score does not help: a four-family core scores lower on all four hazard targets — heatwave days, severe days, heat load and the longest event — in sample and out of sample (held-out heat load 0.72 against 0.79, longest event 0.77 against 0.83, IMD data; Supplementary Table 11). Out of sample, the core drawn from four 15-year windows keeps a normalised precision of 0.82 on the held-out window with IMD days (0.82 with ERA5-Land), about that of an equal-area zone of the training windows' heatwave days (0.78 and 0.85; difference over the five windows $+0.04 \pm 0.06$ and -0.02 ± 0.06; Fig. 7c; Supplementary Table 12), and in the most recent window it is below it. A core drawn from 1951–1995 captures 42% of 1996–2025 IMD heatwave days, as does a persistence zone of the same area (42%), against 50% for the equal-area zone of the most 1996–2025 heatwave days in ERA5-Land (53% for the IMD optimum; Supplementary Table 13). The core is robust to the block length, the season and the definition (Jaccard 0.88–0.95 with the main core) but depends on the quantile cut and the dataset (0.69 for the top tercile, 0.74 with raw ERA5-Land); the rule of the study plan keeps only 10.6% of the lowland (Fig. 7d; Supplementary Table 14).

Table 1 | Zones evaluated as decision products, 1951–2025: area (% of the lowland), precision (capture efficiency: share of heatwave days / share of area), precision normalised by the best zone of the same area, and recall of heatwave days and of severe heatwave days, with ERA5-Land (E) and IMD (I) heatwave days.

Zone	Area %	Prec. E	Prec. I	Norm. E	Norm. I	Recall E	Recall I	Severe I
IMD 2020 list	74.0	1.27	1.27	0.94	0.96	94%	95%	98%
Occurrence zone	30.8	2.20	2.31	0.95	1.00	68%	75%	71%
Concentration core	19.5	2.53	2.62	0.96	0.97	49%	54%	53%
Robust core	13.4	2.71	2.79	0.95	0.94	36%	39%	39%
Four-family core	17.2	2.56	2.63	0.95	0.94	44%	48%	48%
Hotspot zone (Gi*)	21.8	2.38	2.60	0.93	0.99	52%	59%	55%
≥ 3 heatwave days a year	25.5	2.46	2.36	1.00	0.94	63%	61%	58%
Top score, list's area	74.0	1.34	1.31	1.00	0.99	99%	99%	99%
Top heatwave days, core's area	19.4	2.64	2.54	1.00	0.93	51%	51%	46%

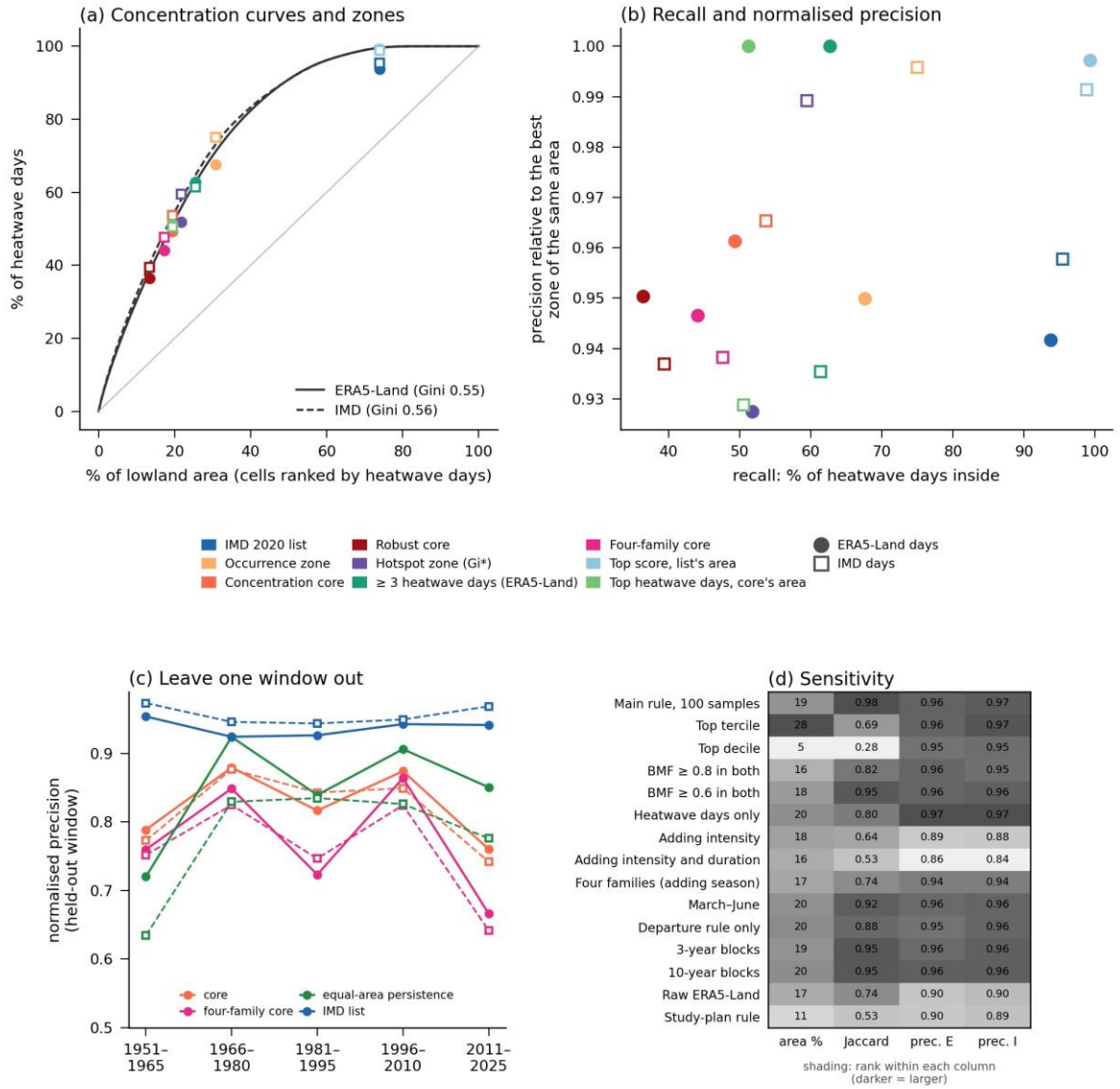

Fig. 7 | The zones as decision products. (a) Concentration (Lorenz) curves of heatwave days against lowland area, cells ranked by heatwave days, with each zone placed by its area and recall (ERA5-Land dots, IMD squares). (b) Recall against precision relative to the best zone of the same area. (c) Normalised precision on each held-out 15-year window of the core drawn from the other four windows, the four-family core, an equal-area persistence zone of the training windows' heatwave days and IMD's list (solid: ERA5-Land days; dashed: IMD days). (d) Sensitivity of the core: area (% of the lowland), Jaccard overlap with the main core and normalised precision with ERA5-Land (E) and IMD (I) days; the first row reruns the main rule with fewer samples.

Change of the core between periods

In IMD, which carries the change, the core of 1996–2025 kept 65% of the 1951–1980 core (Jaccard 0.50); it gained 7.9% of the lowland, mostly in West Rajasthan, East Rajasthan and Vidarbha, and lost 8.8%, mostly in Gangetic West Bengal, Bihar, Jharkhand and Odisha (Fig. 8a). Its centroid moved 259 km west-northwest, more than the shift between two resamples of the same 30-year period (95th percentile 177 km; $p = 0.015$), and 99% of the resampled shifts point within 45° of that bearing. With both datasets the core moved 337 km ($p = 0.005$) and with ERA5-Land alone 286 km ($p = 0.010$), all to the west (Fig. 8b,d; Supplementary Table 15). The change depends on the early record: from 1966–1995

to 1996–2025 the core moved 146 km in IMD (p = 0.16) and 158 km with both datasets (p = 0.20), in the same direction but within the resampling noise. The change is a reshaping — gains in Rajasthan, losses in the east — rather than the displacement of one region. Crossing ERA5-Land's level with IMD's trend shows the same pattern (Fig. 8c): cells with many heatwave days and a rise lie in Rajasthan and western Madhya Pradesh, and those with many and a fall in the east.

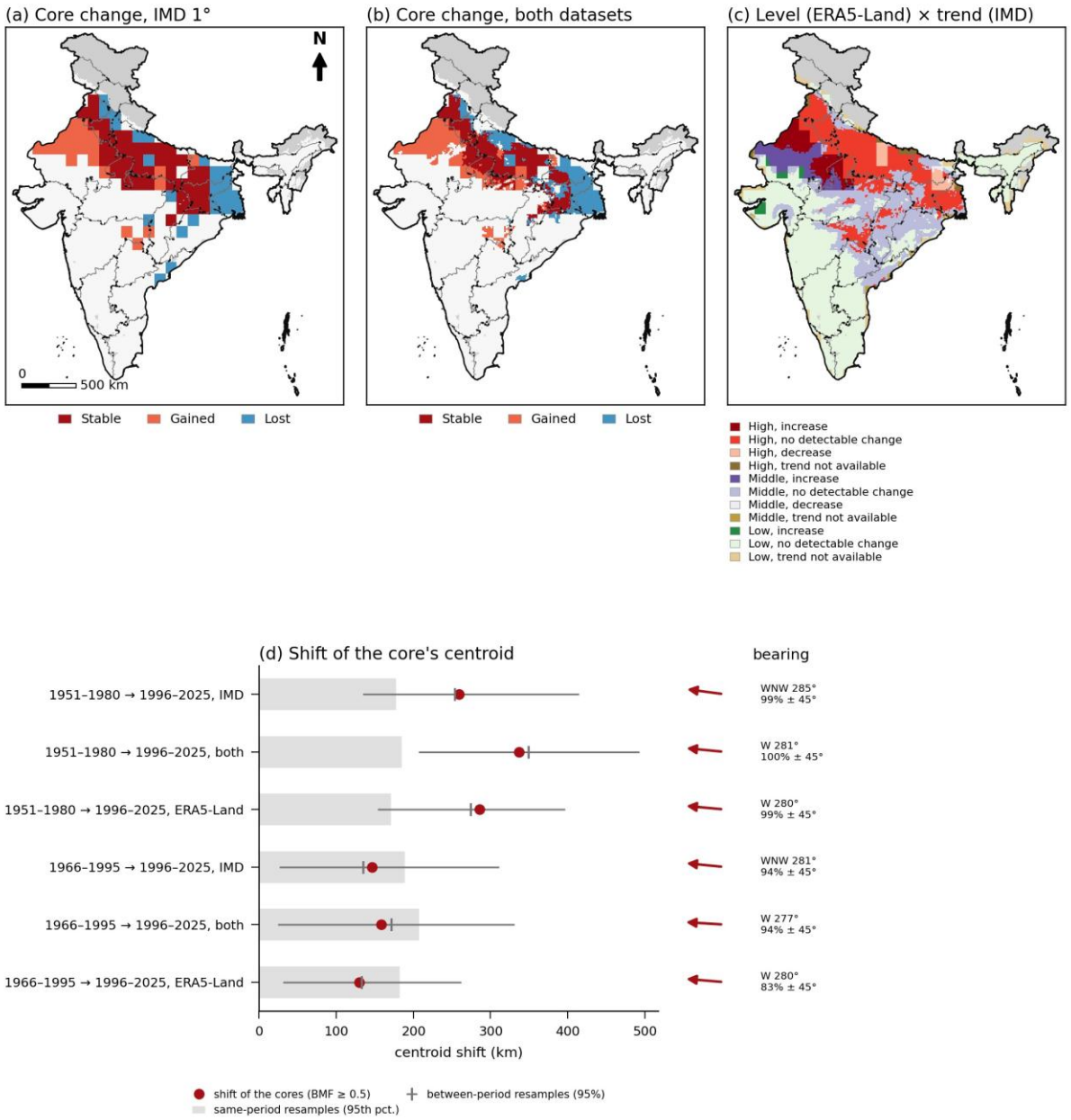

Fig. 8 | Change of the core and hazard-trend classes. (a) Cells in the core of IMD 1° alone and (b) of both datasets (bootstrap membership ≥ 0.5) in both 1951–1980 and 1996–2025 (stable), only in the later period (gained) or only in the earlier one (lost). (c) Level of heatwave days (trend-aligned ERA5-Land, 1951–2025; low < 1, middle 1–3, high ≥ 3 a year) crossed with the trend of the IMD 1° parent cell (Hamed–Rao test, q < 0.10; otherwise no detectable change; grey: the parent is not an IMD lowland cell). (d) Shift of the cores' area-weighted centroid (dots) by period pair and dataset, against the median and 95% range of 100 between-period resamples (whiskers) and the 95th percentile of shifts between two resamples of the same period (grey bar, the noise floor); arrows: bearing (north up), with the share of resampled bearings within 45°. Survey of India outline.

Discussion

Heatwave hazard in India's lowland is a continuum with a weak two-regime structure, and the reporting regions used for it do not follow that structure: IMD's subdivisions and the Köppen–Geiger groups capture the pattern of heatwave days less well than random regions of the same size, while IMD's four homogeneous regions and the Core Heat Wave Zone split do better for heatwave days but not for intensity or duration. The two regimes — more frequent, longer and more intense heatwaves on the Indo-Gangetic plain and in the east, fewer, shorter and milder ones over Madhya Pradesh, Rajasthan, Telangana and Gujarat — divide a severity gradient. They are regimes of places rather than types of events, do not correspond to the two circulation-defined heatwave types over north-central India and the east coast[12], and location predicts them as well as the covariates do.

The Core Heat Wave Zone list should be judged by what it is: a coverage zone. For its size it captures almost as many heatwave days as any zone could, so its breadth is not a defect. What the list cannot provide is a concentration tier, a statement of uncertainty or a way to be updated. The tiered product supplies all three: an occurrence zone for where heatwave preparedness is needed every few years, a core of the most frequent heatwaves with bootstrap membership that users can threshold, and district summaries that place each tier in the units that heat action plans use[5,6]. Frequency alone draws a better core than a composite of frequency, intensity, duration and season, even when the core is judged on heat load or the longest event: the composite adds cells further east, in Chhattisgarh and East Uttar Pradesh, where events are intense but less frequent. Out of sample the core does about as well as a zone drawn from past heatwave days, so its value lies in requiring agreement between two datasets and in stating membership uncertainty, not in forecast skill.

Three findings concern how heatwave criteria behave on grids. The plains rule of 45 °C triggers a large share of heatwave days in Rajasthan and Vidarbha, where departures are small, so an intensity measured as departure from normal would rank the hottest regions as mild; measuring intensity as the excess over the threshold that triggered the day removes that artefact. The terrain floors create steps that are not climate signals: in ERA5-Land, heatwave days rise from 0.10 a year at 900–1,000 m to 2.26 at 1,000–1,100 m, where the 30 °C hill floor starts, and fall from 0.84 at 40–50 km from the sea to 0.59 at 50–60 km, where the 37 °C coastal floor ends (Supplementary Table 16); hills were therefore left out, and the coastal step remains in the zones. And percentile-based heatwave days rise in the peninsula where IMD-criterion days do not, so the definition, and the grid against the station scale, decide whether the south appears as an emerging heatwave region[9,10].

The approach has limits. The aligned ERA5-Land follows IMD's monthly mean trends but not its heatwave-day trends, so change was taken from IMD, whose 1° grid is interpolated from a few hundred stations[20,22]; the two datasets also differ in the 0.1° and 1° scales at which thresholds are crossed[23], and the shift of the core rests on the early decades. The zones describe dry daytime heat; humid and night-

time heat, which dominate mortality on the coasts, need their own products. No station validation of grid-cell heatwave days was possible with open data, no impact data such as heat mortality were available to validate the zones, and the published station and district zonations[14,15] were not available as data for a map-to-map comparison. The rules of the core were fixed after a first analysis, which is why the main alternatives are reported; the normal period and a percentile-based core were not varied. With these caveats, India's heatwave zoning can move from a list to an uncertainty-aware geospatial product: a coverage tier, a concentration core with membership frequencies, and district summaries, each recomputed with the same rules as the record grows.

Methods

The analysis has six steps, from hazard surfaces to change and planning units, each checked against baselines and alternative datasets (Fig. 2).

Study area and terrain classes

India's lowland — cells below 1,000 m, including the Deccan plateau — is the study domain (Fig. 1). The 0.1° grid has 28,933 land cells; cells are classed as hills (mean elevation ≥ 1,000 m), coast (within 50 km of the sea) or plains, the classes named in IMD's heatwave criteria[24], with cut-offs of this study. The lowland has 25,021 cells (2.85 million km², 87% of India). Hills are not analysed: IMD judges hill stations against a 30 °C floor instead of 40 °C, and applying that floor to every grid cell above 1,000 m creates a step in heatwave days at the cut-off rather than a climate signal. IMD's 1° cells enter when at least half their area lies in India, at least 90% of days are valid and their terrain class is lowland (251 cells). Maps use the Survey of India outline; boundaries imply no position on any disputed area, and disputed areas are not labelled.

Temperature data

Daily maximum temperature (Tmax) for 1951–2025 comes from IMD's 1° grid, interpolated from stations[20,22], and from ERA5-Land at 0.1°[21], taken as the highest hourly value between 10:30 and 16:30 Indian Standard Time. Raw ERA5-Land Tmax drifts cooler than IMD over time (regional heatwave-day trends of −15.6 to −7.7% per decade in raw data), so the main 0.1° dataset is trend-aligned: for each lowland cell and month, the slow drift — a centred 21-year running mean of the difference between the mean of the lowland ERA5-Land cells in each IMD cell and IMD — is removed, and the result is corrected by additive empirical quantile mapping fitted on 1991–2020, the IMD-minus-ERA5-Land difference at 100 quantiles of the 1° fit being interpolated bilinearly and added at each 0.1° cell's own quantile. The alignment fixes monthly-mean trends at 1°, not the tails[25] or the 0.1° detail, and the transfer from a 1° box mean to 0.1° cells lets cells cross fixed thresholds more often than IMD's smoothed values[23]; the quantile-mapped and raw versions are robustness checks.

Covariates, region layers and boundaries

Covariates are elevation and coast distance, the irrigated share of each cell for 2000–2015[26] and the 1991–2020 rainfall climatology of IMD's 0.25° grid[27,28]. Region layers (Supplementary Fig. 3) are IMD's meteorological subdivisions[29,30], IMD's four homogeneous regions, Köppen–Geiger groups for 1991–2020[31] and the 2020 Core Heat Wave Zone[1]; districts are Survey of India boundaries with Local Government Directory codes.

Heatwave detection on grids

IMD's criteria[5,24] are applied to every cell: a day qualifies when Tmax reaches the terrain floor (40 °C plains, 37 °C coast) and either departs at least 4.5 °C from the 1991–2020 calendar-day normal (15-day smoothing) or, on the plains, reaches 45 °C; severe days depart more than 6.4 °C or reach 47 °C. Three adaptations are this study's: a heatwave is a run of at least two qualifying days in the cell, where IMD declares one when two stations of a subdivision qualify on two consecutive days; the season is March–September; and the severe level is also applied on the coast. A percentile definition (at least three consecutive days above the calendar-day 90th percentile) and March–June and departure-only versions are sensitivity tests.

Metric families

For every cell and year the analysis uses frequency (heatwave days, events, severe heatwave days), intensity, duration (mean and longest event) and season (first and last heatwave day and the span between them), following the aspects of the heatwave framework[32] with season timing and severe-day counts added. Intensity is the excess of Tmax over the threshold that the day had to reach, max(floor, min(normal + 4.5 °C, 45 °C)) on the plains and max(floor, normal + 4.5 °C) on the coast, so that it is non-negative on every heatwave day whichever rule triggered it; its mean and peak per year are used. Heatwave days are also split into those meeting the departure rule and those meeting only the 45 °C rule. Conditional metrics are averaged over years with a heatwave, and only over heatwave-prone cells (a heatwave in at least 10 of the 75 years).

Region layers, trends and random-partition nulls

For each layer and unit, area-weighted annual series are trended with Sen slopes[33] and the Hamed–Rao modified Mann–Kendall test[34,35], with a 95% interval from the corrected variance and Benjamini–Hochberg control within each layer and metric[36,37]. The between-unit share of the area-weighted variance of per-cell climatology (η^2) measures how much of the hazard pattern a layer captures. Because η^2 grows with the number of units, each layer is compared with 50 random compact partitions of the same lowland into the same number of regions (k-means on cell coordinates from random starts). Whether trends differ between units is tested with the van Belle–Hughes statistic[38,39], the spread of the units' Hamed–Rao Z values (degrees of freedom: units − 1), against a null from the units' detrended

residuals resampled in 5-year blocks shared by all units[40,41]; this tests 'no trend anywhere', so a rejection shows that trends are present in some units, not that they differ; units need heatwave days in at least 20 years, and the false discovery rate is controlled ($q < 0.10$) over all 40 tests. Onset is also trended net of frequency, as the residual after regression on $\log(1 + \text{heatwave days})$, because an earlier first day follows from more heatwave days; these trends are controlled over the subdivisions tested in the same way.

Hazard-versus-trend classes

Each cell's level class comes from its 1951–2025 mean heatwave days (low < 1, middle 1–3, high ≥ 3 per year) and its trend class from the Hamed–Rao test of annual heatwave days (increase or decrease where the false-discovery-rate $q < 0.10$; otherwise 'no detectable change', which is absence of evidence). Because trend-aligned ERA5-Land heatwave-day trends do not follow IMD's, each 0.1° cell takes its level from ERA5-Land and its trend from its IMD parent cell; cells whose parent is not an IMD lowland cell are classed 'trend not available', and the cell's own trend is kept as a check, with Cohen's kappa for the agreement. Level and change are taken from the same period to avoid regression to the mean[42], and each cell's minimum detectable trend at 80% power ((1.96 + 0.84) standard errors of the least-squares slope) is reported.

Heatwave regimes

Heatwave-prone cells are clustered by the 1951–2025 climatology of the four families (square-root transform of counts, robust scaling, each family given total weight one as a design choice so that correlated frequency metrics do not dominate) with area-weighted k-means; the other lowland cells form a rare-heatwave class. The clusters are regimes of places, not types of events. For $k = 2–8$ the years are resampled 100 times with a circular block bootstrap (5-year blocks)[43], clusters are matched to the reference by the Hungarian algorithm[44], and the mean Jaccard similarity of each regime is recorded, adapting Hennig[45]; the chosen k is the largest whose every regime keeps a mean Jaccard of at least 0.75, otherwise the most stable. Silhouette[46], Calinski–Harabasz[47], Davies–Bouldin[48] and gap[49] indices are reported for $k = 2–10$, and the silhouette is compared with Gaussian and Gaussian-copula surrogates of the same covariance, which have no cluster structure[50]; silhouettes of 0.26–0.50 indicate weak structure that may be artificial[51]. Robustness is the adjusted Rand index[52] against $k \pm 1$, a Gaussian mixture[53], Ward clustering[54], the two halves of the record, the percentile definition, each family left out, the other datasets and IMD's own regimes, and HDBSCAN[55] is run over a range of settings.

Explaining the regimes

Predicting the regimes from the metrics that defined them would be circular[56], so they are predicted from external covariates with random forests[57], on plains cells only, because coast distance sets the coastal criterion. Rainfall co-varies with heatwaves through pre-monsoon showers and is treated as a co-variate, not a driver. Geography-only baselines (a random forest on latitude and longitude and a 15-nearest-neighbour classifier) set the bar. Cross-validation holds out spatial blocks[58–60] of 2°, of 5° and of the

empirical range of the regime pattern (the distance at which two cells are no more likely to share a regime than distant cells); the blocks are dealt to five folds in random order, each design is repeated over ten random offsets of the block grid, and the mean and 95% range of held-out balanced accuracy are reported with the number of blocks and the largest fold's share of cells. Importance is the drop in held-out balanced accuracy when a group of related covariates is permuted, under 5° blocks[61,62]; it describes the fitted forest, not a cause.

Tiered heatwave zones

Three zones answer different planning questions. The occurrence zone holds cells with a heatwave in at least one year in three in both datasets (coverage). The concentration core ranks cells by a frequency score, the mean of the area-weighted percentile ranks of heatwave days, heatwave events and severe heatwave days, and keeps the top quartile of the lowland area; the bootstrap membership frequency (BMF) of a cell is the share of 300 circular block bootstrap samples of the years in which it is in the top quartile, a stability frequency rather than a calibrated probability. The core holds cells with a BMF of at least 0.5 in both IMD (through the 1° parent) and trend-aligned ERA5-Land, and the robust core cells with at least 0.9 in both. The hotspot zone holds cells whose Getis–Ord Gi∗[63,64] of heatwave days is significant (one-sided, Benjamini–Hochberg $q < 0.05$) in both datasets, with binary weights within 100 km at 0.1° and the eight neighbours at 1°; spatial autocorrelation makes Gi∗ significance liberal, so the hotspot zone is a comparison, not a test. The rules were set after a first analysis of these data: hills were removed after they entered the core through the 30 °C floor; a four-family score (frequency, intensity, duration and season) was replaced by the frequency score after it scored lower on every hazard target, and is reported as an alternative; and the rule of the study plan (top quartile in at least four of five 15-year windows) is a sensitivity test.

Evaluating zones as decision products

Each zone is judged, with ERA5-Land and with IMD data, on four hazard targets: heatwave days, severe heatwave days, heat load (heatwave days times their mean excess over the threshold, in degree-days per year) and the longest event. Precision is the capture efficiency (share of the target inside the zone divided by the zone's share of area); because precision falls with area, it is also divided by that of the best possible zone of the same area (cells ranked by the target, the 'oracle'); recall is the share of the target inside. Concentration (Lorenz) curves[65] and Gini coefficients summarise how unevenly heatwave days are spread. Equal-area alternatives are the top-scoring cells over the list's area and the cells with most heatwave days over the core's area, and a four-family core (the same membership rule applied to the mean rank over frequency, intensity, duration and season, each family with weight one) tests whether a composite score adds anything. Out-of-sample skill is tested by leaving each 15-year window out, drawing the cores from the other four with the full rule and judging them on the held-out window against an equal-area persistence zone and the list, and by 1951–1995 cores judged on 1996–2025 against the

equal-area zone of the most 1996–2025 heatwave days. A sensitivity matrix varies the quantile cut, the BMF threshold, the family weights, the season, the definition, the block length and the dataset, reporting the zone's area, its Jaccard overlap with the main core and its normalised precision; the family weights are varied by adding intensity, duration and season in turn; the main rule is also rerun with 100 instead of 300 samples to show the Monte-Carlo noise.

Change and planning units

The full rule is applied to 1951–1980 and 1996–2025 (and 1966–1995) in IMD alone, which carries the change, in both datasets and in ERA5-Land alone; the cells gained, lost and retained, the Jaccard overlap and the shift and bearing of the area-weighted centroid are reported. Because a distance cannot be negative, resampling noise alone produces a shift, so the shift is compared with a no-change null: the shift between the top-quartile zones of two independent circular block bootstrap samples of the same 30-year period (100 pairs per period). The between-period shifts of 100 single-sample zones give the spread of the shift and of its bearing. Every product is summarised for each district and subdivision as the share of its lowland area. Zones are distributed as a GeoPackage of 0.1° cells with all products and frequencies.

Software and reproducibility

The analysis uses Python 3.12 with NumPy, pandas, xarray, SciPy, scikit-learn, GeoPandas, Rasterio and pymannkendall[35]; every step is a numbered script with fixed random seeds, and every number in this paper is read from the scripts' output tables. The authors used an AI assistant (Claude, Anthropic) to help write analysis code, check references and edit the text; the authors designed the study, reviewed every step and take full responsibility for the content.

Data availability

IMD gridded temperature and rainfall can be downloaded from IMD Pune[22,28]; ERA5-Land hourly data from the Copernicus Climate Data Store under the Copernicus licence[66]; IMD subdivision boundaries from IMD[30]; Köppen–Geiger maps from Beck et al.[31]; and irrigation maps from Ambika et al.[26]. The zones (occurrence zone, concentration core with bootstrap membership frequencies, the four-family alternative core, hotspot zone, hazard-trend classes, change classes and regimes) are released as a GeoPackage of 0.1° cells with district and subdivision summaries on Zenodo (https://doi.org/10.5281/zenodo.23735314).

Code availability

All analysis scripts (Python 3.12) are archived on Zenodo with the data (https://doi.org/10.5281/zenodo.23735314).

Acknowledgements

This research received no specific grant from any funding agency in the public, commercial or not-for-profit sectors.

Author contributions

A.S. conceived the study, designed the methodology, curated and processed the data, wrote the analysis code, carried out the analysis, prepared the figures and wrote the original draft. V.C.L. contributed to the methodology and the interpretation of the results and reviewed and edited the manuscript. G.S.S. contributed to the literature review and the interpretation of the zones for planning, and reviewed and edited the manuscript. All authors read and approved the final manuscript.

Competing interests

A.S. is the founder, Chief Executive Officer and Managing Director of Globeir Private Limited, which funded this work. V.C.L. and G.S.S. declare no financial or non-financial competing interests.

References

1. India Meteorological Department. Seasonal outlook for temperatures during April to June, 2020. Press release, 30 March 2020 (IMD, 2020). Archived at http://web.archive.org/web/20260301162239/https://mausam.imd.gov.in/backend/assets/press_release_pdf/Seasonal_Outlook_for_Temperatures_during_April_to_June,_2020.pdf (accessed 28 October 2026).
2. Pai, D. S., Srivastava, A. K. & Nair, S. A. Heat and cold waves over India. in *Observed Climate Variability and Change over the Indian Region* (eds Rajeevan, M. N. & Nayak, S.) 51–71 (Springer Geology, Springer, 2017).
3. Pai, D. S., Nair, S. A. & Ramanathan, A. N. Long term climatology and trends of heat waves over India during the recent 50 years (1961-2010). *Mausam* **64**, 585–604 (2013).
4. India Meteorological Department. Updated seasonal outlook for the hot weather season (April to June) 2026 and monthly outlook for April 2026 for the rainfall and temperature. Press release, 31 March 2026 (IMD, 2026). https://internal.imd.gov.in/press_release/20260331_pr_4853.pdf (accessed 28 October 2026).
5. National Disaster Management Authority. *National guidelines for preparation of action plan – prevention and management of heat wave*. Government of India, New Delhi (2019). https://ndma.gov.in/sites/default/files/PDF/Guidelines/heatwaveguidelines.pdf (accessed 27 October 2026).
6. Pillai, A. V. & Dalal, T. *How is India adapting to heatwaves? An assessment of heat action plans with insights for transformative climate action*. Centre for Policy Research, New Delhi (2023). https://cprindia.org/wp-content/uploads/2023/03/Heat-Report_Final_27March-23.pdf (accessed 28 October 2026).
7. Rohini, P., Rajeevan, M. & Srivastava, A. K. On the Variability and Increasing Trends of Heat Waves over India. *Sci. Rep.* **6**, 26153 (2016).
8. Singh, S., Mall, R. K. & Singh, N. Changing spatio-temporal trends of heat wave and severe heat wave events over India: An emerging health hazard. *Int. J. Climatol.* **41**, E1831–E1845 (2021).
9. Tyagi, N., Dube, A., Lakshmi, S., Dutta, S. & Srivastava, A. Shifting of the Zone of Occurrence of Extreme Weather Event—Heat Waves. *Int. J. Climatol.* **45**, e8856 (2025).
10. Das, J. & Pillai, P. A. Mechanism driving pre-monsoon heat waves over southeast and Eastern regions of India. *Clim. Dyn.* **64**, 387 (2026).
11. Banerjee, S., Padmakumari, B. & Ramana, M. V. Intensification and spatial shifts of heatwave hotspot across India under climate and ENSO influences with health risk assessment. *Sci. Rep.* **16**, 8437 (2026).

12. Ratnam, J. V., Behera, S. K., Ratna, S. B., Rajeevan, M. & Yamagata, T. Anatomy of Indian heatwaves. *Sci. Rep.* **6**, 24395 (2016).

13. Mohseni, U., Mittal, S., Ghodichore, N. & Vinnarasi, R. Heat-humidity driven heatwave extremes over India: dry–moist heatwaves and their intraseasonal modulation. *Clim. Dyn.* **64**, 374 (2026).

14. Srivastava, A., Mohapatra, M. & Kumar, N. Hot weather hazard analysis over India. *Sci. Rep.* **12**, 19768 (2022).

15. V, S., Suresh, N., Mondal, A. & Mishra, T. A stitch in time: district scale heatwave hazard, vulnerability and risk assessment in India. *Environ. Res. Commun.* **8**, 025022 (2026).

16. Stefanon, M., D'Andrea, F. & Drobinski, P. Heatwave classification over Europe and the Mediterranean region. *Environ. Res. Lett.* **7**, 014023 (2012).

17. Suli, S., Barriopedro, D., García-Herrera, R. & Rusticucci, M. Regionalisation of heat waves in southern South America. *Weather Clim. Extrem.* **40**, 100569 (2023).

18. Yao, J. et al. Summer Regional Pentad Heat Wave in Eastern China and Their Possible Causes. *Front. Earth Sci.* **8**, 598027 (2020).

19. Yu, Y., Shao, Q., Lin, Z. & Kang, I. Characteristics Analysis and Synoptic Features of Event-Based Regional Heatwaves Over China. *J. Geophys. Res. Atmos.* **126**, e2020JD033865 (2021).

20. Srivastava, A. K., Rajeevan, M. & Kshirsagar, S. R. Development of a high resolution daily gridded temperature data set (1969–2005) for the Indian region. *Atmos. Sci. Lett.* **10**, 249–254 (2009).

21. Muñoz-Sabater, J. et al. ERA5-Land: a state-of-the-art global reanalysis dataset for land applications. *Earth Syst. Sci. Data* **13**, 4349–4383 (2021).

22. India Meteorological Department. *Yearly gridded maximum and minimum temperature (1.0° × 1.0°) data, 1951 onwards*. IMD Pune (n.d.). https://www.imdpune.gov.in/cmpg/Griddata/Max_1_Bin.html (accessed 28 October 2026).

23. Maraun, D. Bias Correction, Quantile Mapping, and Downscaling: Revisiting the Inflation Issue. *J. Clim.* **26**, 2137–2143 (2013).

24. India Meteorological Department. *Frequently asked questions on heat wave* (n.d.). https://mausam.imd.gov.in/pdfs/heatcolduser/FAQ_heat_wave.pdf (accessed 28 October 2026).

25. Cannon, A. J., Sobie, S. R. & Murdock, T. Q. Bias Correction of GCM Precipitation by Quantile Mapping: How Well Do Methods Preserve Changes in Quantiles and Extremes? *J. Clim.* **28**, 6938–6959 (2015).

26. Ambika, A. K., Wardlow, B. & Mishra, V. Remotely sensed high resolution irrigated area mapping in India for 2000 to 2015. *Sci. Data* **3**, 160118 (2016).

27. Pai, D. S., Rajeevan, M., Sreejith, O. P., Mukhopadhyay, B. & Satbha, N. S. Development of a new high spatial resolution (0.25° × 0.25°) long period (1901-2010) daily gridded rainfall data set over India and its comparison with existing data sets over the region. *Mausam* **65**, 1–18 (2014).

28. India Meteorological Department. *High spatial resolution (0.25° × 0.25°) long period daily gridded rainfall data set over India*. IMD Pune (n.d.). https://www.imdpune.gov.in/cmpg/Griddata/Rainfall_25_Bin.html (accessed 28 October 2026).

29. Kelkar, R. R. & Sreejith, O. P. Meteorological sub-divisions of India and their geopolitical evolution from 1875 to 2020. *Mausam* **71**, 571–584 (2020).

30. India Meteorological Department. *Meteorological subdivision boundaries* (GeoJSON) (n.d.). https://mausam.imd.gov.in/imd_latest/contents/district_shapefiles/sd_boundary.json and https://mausam.imd.gov.in/imd_latest/contents/district_shapefiles/sd_boundary_rainfall.json (accessed 28 October 2026).

31. Beck, H. E. et al. High-resolution (1 km) Köppen-Geiger maps for 1901–2099 based on constrained CMIP6 projections. *Sci. Data* **10**, 724 (2023).

32. Perkins, S. E. & Alexander, L. V. On the Measurement of Heat Waves. *J. Clim.* **26**, 4500–4517 (2013).

33. Sen, P. K. Estimates of the Regression Coefficient Based on Kendall's Tau. *J. Am. Stat. Assoc.* **63**, 1379–1389 (1968).

34. Hamed, K. H. & Ramachandra Rao, A. A modified Mann-Kendall trend test for autocorrelated data. *J. Hydrol.* **204**, 182–196 (1998).

35. Hussain, M. & Mahmud, I. pyMannKendall: a python package for non parametric Mann Kendall family of trend tests. *J. Open Source Softw.* **4**, 1556 (2019).

36. Benjamini, Y. & Hochberg, Y. Controlling the False Discovery Rate: A Practical and Powerful Approach to Multiple Testing. *J. R. Stat. Soc. B* **57**, 289–300 (1995).

37. Wilks, D. S. "The Stippling Shows Statistically Significant Grid Points": How Research Results are Routinely Overstated and Overinterpreted, and What to Do about It. *Bull. Am. Meteorol. Soc.* **97**, 2263–2273 (2016).

38. van Belle, G. & Hughes, J. P. Nonparametric Tests for Trend in Water Quality. *Water Resour. Res.* **20**, 127–136 (1984).

39. Gilbert, R. O. *Statistical Methods for Environmental Pollution Monitoring* (Van Nostrand Reinhold, 1987).

40. Douglas, E. M., Vogel, R. M. & Kroll, C. N. Trends in floods and low flows in the United States: impact of spatial correlation. *J. Hydrol.* **240**, 90–105 (2000).

41. Wilks, D. S. Resampling Hypothesis Tests for Autocorrelated Fields. *J. Clim.* **10**, 65–82 (1997).

42. Barnett, A. G., van der Pols, J. C. & Dobson, A. J. Regression to the mean: what it is and how to deal with it. *Int. J. Epidemiol.* **34**, 215–220 (2005).

43. Politis, D. N. & Romano, J. P. A circular block-resampling procedure for stationary data. in *Exploring the Limits of Bootstrap* (eds LePage, R. & Billard, L.) 263–270 (Wiley, 1992).

44. Kuhn, H. W. The Hungarian method for the assignment problem. *Nav. Res. Logist. Q.* **2**, 83–97 (1955).

45. Hennig, C. Cluster-wise assessment of cluster stability. *Comput. Stat. Data Anal.* **52**, 258–271 (2007).

46. Rousseeuw, P. J. Silhouettes: A graphical aid to the interpretation and validation of cluster analysis. *J. Comput. Appl. Math.* **20**, 53–65 (1987).

47. Caliński, T. & Harabasz, J. A dendrite method for cluster analysis. *Commun. Stat.* **3**, 1–27 (1974).

48. Davies, D. L. & Bouldin, D. W. A Cluster Separation Measure. *IEEE Trans. Pattern Anal. Mach. Intell.* **PAMI-1**, 224–227 (1979).

49. Tibshirani, R., Walther, G. & Hastie, T. Estimating the Number of Clusters in a Data Set Via the Gap Statistic. *J. R. Stat. Soc. B* **63**, 411–423 (2001).

50. Şenbabaoğlu, Y., Michailidis, G. & Li, J. Z. Critical limitations of consensus clustering in class discovery. *Sci. Rep.* **4**, 6207 (2014).

51. Kaufman, L. & Rousseeuw, P. J. *Finding Groups in Data: An Introduction to Cluster Analysis* (Wiley, 1990).

52. Hubert, L. & Arabie, P. Comparing partitions. *J. Classif.* **2**, 193–218 (1985).

53. Fraley, C. & Raftery, A. E. Model-Based Clustering, Discriminant Analysis, and Density Estimation. *J. Am. Stat. Assoc.* **97**, 611–631 (2002).

54. Ward, J. H. Hierarchical Grouping to Optimize an Objective Function. *J. Am. Stat. Assoc.* **58**, 236–244 (1963).

55. Campello, R. J. G. B., Moulavi, D. & Sander, J. Density-based clustering based on hierarchical density estimates. in *Advances in Knowledge Discovery and Data Mining*, Lecture Notes in Computer Science Vol. 7819, 160–172 (Springer, 2013).

56. Kriegeskorte, N., Simmons, W. K., Bellgowan, P. S. F. & Baker, C. I. Circular analysis in systems neuroscience: the dangers of double dipping. *Nat. Neurosci.* **12**, 535–540 (2009).

57. Breiman, L. Random Forests. *Mach. Learn.* **45**, 5–32 (2001).

58. Roberts, D. R. et al. Cross-validation strategies for data with temporal, spatial, hierarchical, or phylogenetic structure. *Ecography* **40**, 913–929 (2017).

59. Ploton, P. et al. Spatial validation reveals poor predictive performance of large-scale ecological mapping models. *Nat. Commun.* **11**, 4540 (2020).

60. Valavi, R., Elith, J., Lahoz-Monfort, J. J. & Guillera-Arroita, G. blockCV: an R package for generating spatially or environmentally separated folds for k-fold cross-validation of species distribution models. *Methods Ecol. Evol.* **10**, 225–232 (2019).

61. Strobl, C., Boulesteix, A.-L., Kneib, T., Augustin, T. & Zeileis, A. Conditional variable importance for random forests. *BMC Bioinformatics* **9**, 307 (2008).

62. Gregorutti, B., Michel, B. & Saint-Pierre, P. Correlation and variable importance in random forests. *Stat. Comput.* **27**, 659–678 (2017).

570 63. Getis, A. & Ord, J. K. The Analysis of Spatial Association by Use of Distance Statistics. *Geogr. Anal.* **24**, 189–206
571 (1992).
572 64. Ord, J. K. & Getis, A. Local Spatial Autocorrelation Statistics: Distributional Issues and an Application. *Geogr.*
573 *Anal.* **27**, 286–306 (1995).
574 65. Lorenz, M. O. Methods of Measuring the Concentration of Wealth. *Publ. Am. Stat. Assoc.* **9**, 209–219 (1905).
575 66. Muñoz Sabater, J. ERA5-Land hourly data from 1950 to present. Copernicus Climate Change Service Climate
576 Data Store https://doi.org/10.24381/cds.e2161bac (2019).

Supplementary Files

This is a list of supplementary files associated with this preprint. Click to download.

- HeatHazardZoningSupplementaryInformation.docx